High-ratiO partiaL proteolysiS with carriER proteome (HOLSER) Enables Global Structure Profiling and Site-resolved Elucidation of Ligand–Protein Interactions

Xuepei Zhang[1,2,3], Bohdana Sokolova[1], Zhaowei Meng[1,2,3], Hassan Gharibi[1,2,3], Massimiliano Gaetani[1,2,3*], Roman A. Zubarev[1, 2, 3, 4*]

[1] Division of Chemistry I, Department of Medical Biochemistry and Biophysics, Karolinska Institutet, SE-17 177 Stockholm, Sweden

[2] Chemical Proteomics Unit, Science for Life Laboratory (SciLifeLab), Stockholm, Sweden

[3] Chemical Proteomics, Swedish National Infrastructure for Biological Mass Spectrometry (BioMS), Stockholm, Sweden

[4] Department of Pharmacological & Technological Chemistry, I.M. Sechenov First Moscow State Medical University, Moscow, Russia

* Correspondence and requests for materials should be addressed to M.G and R.A.Z.

(email: massimiliano.gaetani@ki.se; roman.zubarev@ki.se)

Abstract

Understanding how cellular proteins interact with their environment, including endogenous and exogeneous molecules, is critical for elucidating mechanisms of cellular regulation and drug action. Proteolysis-based stability profiling methods such as peptide-centric local stability assay (PELSA) offer peptide-level resolution of ligand-induced conformational changes but are limited by modest proteome coverage and depth, as well as high variability. To overcome these limitations, we developed high ratio partial proteolysis with carrier proteome (HOLSER), an efficient workflow that combines high enzyme-to-substrate ratio with extended digestion time for low peptide yield variability and tandem mass tag (TMT)-based multiplexing that includes full digests for enhanced proteome depth and sequence coverage as well as precision of abundance measurements. We demonstrate HOLSER's capabilities across diverse usage cases, including global proteome structure profiling, proof-of-principle methotrexate target elucidation, kinase target mapping with staurosporine, and high-resolution analysis of the FKBP–mTOR complex response to rapamycin. HOLSER reveals domain-specific stabilization and identifies peptides in direct contact with ligands, providing a powerful and scalable platform for simultaneous probing structural changes at the scale of the whole proteome, individual protein domains and specific binding sites.

Introduction

Identifying and characterizing protein native structures and their changes upon protein–ligand interactions is essential for understanding cellular signaling, the molecular basis of disease and drug mechanisms. Traditional approaches such as thermal shift assays and affinity-based pull-downs often lack the resolution or throughput required to profile complex proteomes under physiologically relevant conditions. In recent years, proteolysis-based stability profiling methods like limited proteolysis–mass spectrometry (LiP–MS)[1-3], and peptide-centric local stability assay (PELSA)[4] have emerged as powerful tools to detect ligand-induced conformational changes at the peptide level. These methods rely on limited proteolysis of native proteins, where stabilized regions resist enzymatic cleavage in the presence of a binding ligand, allowing downstream quantification of the ligand-induced changes via mass spectrometry.

Methods such as PELSA where the use of lower-grade trypsin at a high enzyme-substrate ratio (1:2) in combination with a very short digestion time opened way for scalable structural analysis at the proteome level and demonstrated spectacular results in selected cases. But despite these significant promises, the technique showed some critical limitations. Due to the shallow digestion PELSA is hampered by modest proteome depth and sequence coverage, which significantly limits the generality of the analysis. This is because the critical for drug target elucidation transition from the peptides to the protein level is based in PELSA on the behavior of a single peptide. Furthermore, due to the short, one-minute digestion time the approach may also suffer from stochastic quantification variability, particularly for low-abundance proteins and transient interactions. These shortcomings limit the technique applicability in high-throughput ligand screening and domain-level interaction mapping.

To address these challenges, we developed HOLSER — an optimized workflow for ligand-induced stability profiling in cell lysate under native conditions (Fig. 1A). Inspired by PELSA to use high enzyme-to-substrate (E/S) ratio of 1:1 (wt/wt) and lower-grade trypsin, HOLSER features several critical differences. First, the digestion time is extended from one to four minutes to improve cleavage uniformity and reduce stochastic variability of the peptide yield. Then, instead of the label-free analysis that suffers almost incurably from the random fluctuations of electrospray current, HOLSER employs the more precise tandem mass tag (TMT)-based quantification, with data-dependent acquisition that is less prone to false positive results that the data-independent acquisition (DIA). Moreover, in the same TNT set partial digests are multiplexed in HOLSER with full (8 h) digest in “carrier” channels. As in single-cell proteomics, the main purpose is to boost sensitivity, especially for low-abundant peptides

that emerge from protected regions, and thus increase the analysis depth (number of quantified peptides and proteins) and average protein sequence coverage. Also, the ratio of the peptide abundances in the partial digest versus full digest provides the "accessibility factor" that is linked to protein tertiary structure. Even though deeper proteome analysis with TMT is achieved by the use of sample fractionation, better precision allows one to reduce the number of replicates from 4 to 3 without losses in statistical power, with an overall win in the instrumental time. Finally, instead of a single "best" peptide, HOLSER use several peptides for determining the target protein, with their p-values combined using Fisher's formula. This provides robust and statistically viable target identification.

In this proof of principle study, we apply HOLSER to verifying known ligand–protein interactions with high spatial resolution. We benchmark HOLSER performance against PELSA in global proteome profiling, staurosporine kinase target deconvolution, and targeted analysis of the FKBP–mTOR complex under rapamycin treatment. The results confirm that, as expected, HOLSER significantly improves proteome depth, protein sequence coverage, and the robustness of ligand-induced stabilization, additionally allowing for domain-level global mapping.

Result

Enhanced Peptide Coverage and Quantification in Native Proteolysis Using HOLSER with TMT-Based Multiplexing

To improve the reproducibility, sensitivity, and depth of coverage in ligand-induced stability profiling, we developed an optimized proteolysis-based proteomics workflow, which we term HOLSER. The method builds on key principles of PELSA but introduces longer digestion time (4 minutes at room temperature) while maintaining a high enzyme-to-substrate (E/S) ratio of 1:1 (wt/wt). This adjustment reduces variability compared to the original 1-minute PELSA digestion and increases the depth of peptide coverage under native conditions (Fig. 1A).

A central feature of HOLSER is the use of TMT-based multiplexing, which enhances peptide detection sensitivity through the inclusion of carrier and control channels (Fig. 1B). Specifically, each TMT set includes: (1) Native lysates (with and without ligand treatment), subjected to short 4-minute digestion. (2) 8-hour native digests, included as carrier channels.

These full digests provide abundant fully tryptic peptides that enhance MS1 signal intensities of overlapping peptides from native digests, thereby boosting the signal of low-abundance

peptides and improving their quantification. This strategy is conceptually similar to the "carrier" approach used in single-cell proteomics[5] but implemented without the need for an external carrier sample.

Box plots showing TMT channel peptide abundances normalized to the full-digest samples (set at 100%) confirmed consistent quantification across the dataset (Fig. 1C). The enhanced signal transmission from the normalizer samples enabled robust quantification of many peptides that would otherwise fall below detection thresholds in conventional PELSA or HT-PELSA workflows.

HOLSER Improves Proteome Coverage and Sensitivity Compared to PELSA

To assess the performance of HOLSER relative to the original PELSA method, we compared the number of identified proteins and peptides, as well as the overall protein sequence coverage in each workflow (Fig. 2A–C).

The protein-level comparison (Fig. 2A) showed a large overlap between the two methods, but HOLSER uniquely identified an additional 3430 proteins not detected by PELSA, reflecting its enhanced sensitivity. Similarly, at the peptide level, HOLSER recovered substantially more peptides, with a total of 139,849 peptides identified, compared to 71,708 peptides in PELSA (Fig. 2B). This improvement in peptide yield translated into notably higher protein sequence coverage. On average, HOLSE achieved 35% sequence coverage, more than double the coverage obtained with PELSA (16.8%) (Fig. 2C). The box plot clearly shows the shift toward higher coverage across nearly all quantified proteins under HOLSER conditions. These improvements are attributed to the longer 4-minute digestion, the inclusion of full-digest carriers, and TMT-based signal enhancement, which together enable more comprehensive peptide detection and more confident identification of ligand-induced stability changes.

HOLSER Reveals Peptide-Resolved Stabilization of DHFR Upon MTX Treatment

To evaluate the ability of HOLSER to capture ligand-induced conformational shifts, we applied the method to lysates treated with methotrexate (MTX) and compared them to DMSO controls across three biological replicates. At the peptide level (Fig. 3A), a volcano plot revealed widespread and statistically significant changes in peptide abundance in response to MTX treatment. Notably, multiple peptides derived from dihydrofolate reductase (DHFR) — the known target of MTX—exhibited strong stabilization, consistent with ligand-induced protection from proteolysis. Peptides were ranked by a combined score (defined as absolute

$\log_2$ fold change × $-\log_{10}$ p-value), which prioritized DHFR-derived peptides among the top candidates (Fig. 3B), underscoring the sensitivity of HOLSER to detect target-specific effects.

At the protein level (Fig. 3C), abundance changes were evaluated by combining the p-values of the top three peptides per protein—selected based on their combined score—using Fisher's method. The protein level results further confirmed that MTX treatment elicited statistically supported changes at the full-protein level, including for DHFR.

Taken together, these data demonstrate that HOLSER captures ligand-induced protein stability changes with high sensitivity and resolution. The peptide-level analysis is particularly informative for detecting local conformational effects, while the integrated protein-level statistics support the broader impact of the ligand on the proteome.

Kinase-targeting Analysis Reveals Enhanced Sensitivity and Domain-Level Resolution by HOLSER

To further demonstrate the capability of HOLSER in profiling kinase-ligand interactions, we analyzed peptide abundance changes upon treatment with the broad-spectrum kinase inhibitor staurosporine[6, 7]. Across the dataset, a total of 8,562 peptides were confidently assigned to kinase proteins based on UniProt annotation. In the PELSA workflow, 22% of kinase-derived peptides exhibited significant abundance changes ($p < 0.05$, t-test, $n = 4$ biological replicates), whereas in HOLSER, this percentage increased substantially to 45.1% ($p < 0.05$, t-test, $n = 3$ biological replicates) (Fig. 4A, B). The distribution of significant peptides per kinase also shifted toward higher percentages in HOLSER compared to PELSA, as shown in the density plot (Fig. 4C), with median values of 41.7% and 18.2%, respectively. These results highlight the improved sensitivity of HOLSER in detecting kinase-specific stability shifts induced by staurosporine.

Volcano plot analysis of peptide-level changes further emphasizes the strong kinase peptide signals detected by HOLSER in staurosporine-treated samples (Fig. 4D). Among the top 50 peptides ranked by a combined score of fold change and significance, 46 peptides are derived from kinases, while the remaining four peptides correspond to non-kinase proteins GFM1, HSP90AA1, CBR1, and ANXA1 (Fig. 4E). Notably, two of these non-kinase proteins, ANXA1 and HSP90AA1, have been previously reported to interact with or be functionally associated with kinase signaling and staurosporine treatment. HSP90AA1, a molecular chaperone, is known to bind and stabilize a wide range of kinases, facilitating their proper folding and function [8, 9]. ANXA1 has also been implicated in signaling pathways that cross-talk with kinase

activities and modulates cellular responses to kinase inhibitors like staurosporine[10, 11]. This observation indicates that HOLSER can effectively profile not only direct ligand binding to kinases but also indirect interactions within the kinase signaling network.

At the protein level, abundance changes upon staurosporine treatment mirrored peptide-level observations, with kinase proteins showing pronounced shifts compared to controls (Fig. 4F). Focusing on CSK[12], a well-characterized kinase, HOLSER identified substantially more peptides covering its kinase domain than PELSA. Nearly all significant peptides were mapped within the kinase domain, with those scoring highest localized around known staurosporine binding sites (Fig. 4G). Structural visualization of the CSK– staurosporine complex[13] (PDB ID: 1BYG) highlighted these regions, supporting HOLSER's capability to provide detailed insights into ligand binding sites and conformational changes upon treatment (Fig. 4H).

Supplementary analyses further underscored HOLSER's enhanced resolution. For DAKP1, a significantly stabilized peptide overlapping kinase binding sites I160 and D161 were detected exclusively by HOLSER (Supplementary Fig. 1A-B), while PELSA failed to detect any DAKP1 peptides. RPS6KA3[14] peptides significantly altered upon treatment localized to both the N-terminal and C-terminal kinase domains; however, peptides clustering in the N-domain were more significant, indicating a stronger staurosporine binding affinity at this site. This domain-specific binding differentiation was not observed in PELSA (Supplementary Fig. 1C). For the molecular chaperone HSP90AA1, the most significant peptides were located in its middle domain, responsible for client protein interactions, further confirming HOLSER's ability to profile indirect ligand interactions (Supplementary Fig. 1D).

Together, these data demonstrate that HOLSER markedly improves kinase target detection, peptide coverage, and domain-level resolution of ligand binding and protein stability changes, providing a powerful tool for dissecting complex protein–ligand interactions in native biological contexts.

HOLSER Enables Enhanced Profiling of FKBP–mTOR Complex Response to Rapamycin

To explore the capacity of HOLSER to resolve ligand-induced stability changes within protein complexes, we applied the method to rapamycin-treated samples. Rapamycin targets FKBP proteins and mTOR, forming a ternary complex critical for mTOR pathway regulation[15, 16]. In HOLSER, volcano plot analysis revealed clear abundance changes at the peptide level for FKBP and mTOR family members upon rapamycin treatment, with 183 out of 439 detected

peptides (41.7%) showing statistically significant shifts ($p < 0.05$, t-test, $n = 3$ biological replicates) (Fig. 5A, C). At the protein level, corresponding changes were also observed (Fig. 5B), with consistent directional trends for the FKBP–mTOR complex components.

To assess how this performance compares to conventional methods, we analyzed similar samples using PELSA. In PELSA, only 254 peptides from FKBP and mTOR proteins were detected, and just 52 (20.5%) of these showed significant abundance changes (Fig. 5D), reflecting lower sensitivity and depth of coverage. These results highlight HOLSER's improved ability to detect ligand-induced conformational changes, particularly in low-abundance or partially folded peptides.

Sequence mapping of FKBP3[17]-derived peptides showed that HOLSER provided broader coverage across the protein and identified multiple significant peptides not detected in PELSA (Fig. 5E). These significant peptides spanned many known binding sites within FKBP3. Notably, the peptide LEIEPEWAYGKK, which showed the most pronounced abundance shift compared with DMSO, includes the residue Y198, located at just 1.76 Å from rapamycin in the FKBP3–rapamycin complex structure[18] (PDB ID: 1PBK) (Fig. 5F). This spatial correlation between proteomic signal and ligand proximity supports the conclusion that HOLSER can not only enhance detection sensitivity but also resolve direct binding interactions with high spatial accuracy.

To further explore the ability of HOLSER to resolve binding-site-level interactions within FKBP family members, we closely examined FKBP5[19]. Among the peptides identified by HOLSER, the most significant was KFDSSHDR, which includes residues D68 and R73—both of which form salt bridges with rapamycin in the FKBP5–rapamycin complex structure[15] (PDB ID: 4DRI) (Supplementary Fig. 2B). Salt bridges play a critical role in molecular recognition due to their strong electrostatic forces and frequent hydrogen bonding components, providing high specificity in ligand binding[20-22]. In contrast, the most significant peptide identified by PELSA in FKBP5 included W90, which participates in hydrophobic interactions with rapamycin. While hydrophobic contacts contribute to binding affinity, they are generally weaker and less specific than salt bridges[23, 24]. These findings emphasize HOLSER's capacity to detect functionally stronger and more specific interactions, enabling high-resolution mapping of binding events that are likely to govern ligand selectivity and efficacy.

In FKBP2[25], significantly stabilized peptides were predominantly located within the PPIase domain, the functional region responsible for peptidyl-prolyl isomerase activity

(Supplementary Fig. 2C). Compared to PELSA, HOLSER not only identified a greater number of FKBP2-derived peptides but also achieved higher sequence coverage across the PPIase domain, enabling more confident detection of ligand-induced stabilization. We also examined FKBP9[26], another member of the FKBP family, to assess domain-level resolution of ligand engagement. HOLSER identified multiple significantly stabilized peptides spanning two of PPIase FKBP domains as well as the EF-hand motifs (Supplementary Fig. 2D). These domains are critical for FKBP9's function in protein folding and calcium binding, respectively. The detection of stability shifts within these regions suggests that rapamycin may engage not only the canonical PPIase sites but also influence conformational dynamics in calcium-sensing EF-hand domains. This observation highlights HOLSER's ability to profile multi-domain interactions and potential allosteric effects induced by ligand binding—features that are difficult to resolve using conventional methods like PELSA, which failed to capture these domain-specific changes in FKBP9. These results further demonstrate the advantage of HOLSER in capturing domain-specific responses and improving sensitivity for functionally relevant regions of target proteins.

Conclusions

We developed HOLSER, a native proteolysis-based proteomics workflow that enables enhanced peptide coverage, improved quantification, and increased sensitivity for detecting ligand-induced protein stability changes. The method combines short digestion under native conditions with a high enzyme-to-substrate ratio, TMT-based multiplexing, and the inclusion of full-digest carrier channels to improve the detectability of low-abundance peptides and increase overall proteome coverage.

Compared to existing approaches, such as PELSA, HOLSER detects a greater number of peptides and proteins, yields higher sequence coverage, and offers improved resolution at both the peptide and protein levels. These advantages support more confident and detailed detection of ligand-induced stability shifts. HOLSER accurately captured methotrexate-induced stabilization of DHFR, revealed widespread and domain-specific effects of staurosporine on kinases, and resolved direct binding events and allosteric effects in the FKBP–mTOR complex in response to rapamycin. The method also identified indirect targets and functionally relevant interaction domains that were not detected using PELSA.

In summary, HOLSER provides a robust and sensitive platform for profiling protein–ligand interactions under native conditions, with broad applications in target engagement studies, drug mechanism-of-action analysis, and proteome-wide conformational profiling.

Methods

Cell culture

Hela cells were kindly provided by colleagues from Karolinska Institutet. Cells were grown in Dulbecco's Modified Eagle's Medium (DEME, Thermo Fisher Scientific 11594446) supplemented with 10% heat-inactivated fetal bovine serum (FBS, Thermo Fisher Scientific 11560636) and 1% penicillin/streptomycin (15140-122, Gibco) in a humidified atmosphere containing 5% CO_2 at 37 ℃.

HOLSER assay

Hela cells were collected and washed with PBS twice. The cells were resuspended in 20mM EPPS buffer at pH 8.2 containing protease inhibitors (Thermo Fisher Scientific 78439) and were subjected to three freeze/thaw cycles to lyse the cells. The protein concentration was measured using a rapid protein quantification assay kit (Pierce 660 nm, Thermo Fisher Scientific) according to the manufacturer's protocol. Then the lysate was diluted to 1mg/mL with the lysis buffer.

50 μL of cell lysates were incubated with 5 μL of the analyte ligand or DMSO for 30 min at 25 °C with three replicates and the final concentration of the ligand was 10 μM for MTX, 10 μM for staurosporine and 2 μM for rapamycin, respectively.

Following ligand incubation, limited proteolysis with native trypsin was carried out at an enzyme-to-substrate ratio of 1:1 (wt/wt) for a total duration of 1 minute. Specifically, 10 μl of trypsin stock (5 mg/ml; Sigma-Aldrich, T1426) was added to 50 μg of protein sample. The mixture was gently and thoroughly mixed for 30 seconds using a multichannel pipette to ensure even distribution. The samples were then incubated at 25 °C for 3 minutes and 30 seconds in an Eppendorf® ThermoMixer® F1.5, shaking at 1,000 rpm. For carrier samples, trypsin digestion was carried out for an extended period of 8 hours to ensure thorough proteolysis. Proteolysis was stopped by adding 165 μl of 8 M guanidine hydrochloride (GdmCl) in 20 mM EPPS buffer (pH 8.2), resulting in a final concentration of 6 M GdmCl.

To perform carbamidomethylation, tris(2-carboxyethyl) phosphine (TCEP) and iodoacetamide (IAA) were added to the digested protein samples to final concentrations of 10 mM and 40 mM, respectively. The mixture was subsequently incubated at 95 °C for 5 minutes to allow for complete alkylation of cysteine residues.

After alkylation, the samples were diluted to a final concentration of 1 M guanidine GdmCl using 20 mM EPPS buffer (pH 8.2). The peptide samples were labelled using 16 TMTpro reagents (Thermo Fisher Scientific, A44520,) according to manufacturer's instructions and the labelling was quenched by 50% hydroxylamine (Thermo Fisher Scientific, 15225753). After multiplexing, the sample was acidified by adding trifluoroacetic acid (TFA) to reach a final concentration of 1%. Peptide samples were desalted using C18 Sep-Pak cartridge prior to LC-MS/MS analysis. The cartridge was first conditioned by washing twice with 1 mL of 100% acetonitrile (ACN), followed by two washes with 1 mL of 0.1% trifluoroacetic acid (TFA) to equilibrate the resin. Acidified peptide samples were then loaded onto the cartridge and washed twice with 5% ACN with 0.1% formic acid (FA) to remove salt and other contaminants. Peptides were eluted using 50% ACN containing 0.1% FA in two steps of 300 µL each. The eluates were collected subsequently dried for further analysis. Dried peptides were fractionated by high-performance liquid chromatography using a Dionex Ultimate 3000 UPLC system (Thermo Fisher Scientific) as previously described. This process generated 48 fractions, which were concatenated by pooling every eight fractions into one, resulting in 12 combined fractions per TMT-multiplexed sample set. These pooled fractions were then subjected to nanoLC-MS/MS analysis following standard shotgun proteomics workflows. For LC-MS/MS analysis, 1 µg of each pooled fraction was injected and analyzed following standard shotgun proteomics workflows.

NanoLC-MS/MS analysis

NanoLC-MS/MS analyses were performed on an Orbitrap Exploris 480 mass spectrometer (Thermo Fisher Scientific). The instrument was equipped with an EASY ElectroSpray source and connected online to an Ultimate 3000 nanoflow UPLC system. The samples were pre-concentrated and desalted online using a PepMap C18 nano-trap column (length - 2 cm; inner diameter - 75 µm; particle size - 3 µm; pore size - 100 Å; Thermo Fisher Scientific) with a flow rate of 3 µL/min for 5 min. Peptide separation was performed on an EASY-Spray C18 reversed-phase nano-LC column (Acclaim PepMap RSLC; length - 50 cm; inner diameter - 2 µm; particle size - 2 µm; pore size – 100 Å; Thermo Scientific) at 55 °C and a flow rate of 300 nL/min. Peptides were separated using a binary solvent system consisting of 0.1% (v/v) FA, 2% (v/v) ACN (solvent A) and 98% ACN (v/v), 0.1% (v/v) FA (solvent B). They were eluted with a gradient of 3–26% B in 97 min, and 26–95% B in 9 min. Subsequently, the analytical column was washed with 95% B for 5 min before re-equilibration with 3% B. The mass spectrometer was operated in a data-dependent acquisition mode. A survey mass spectrum (from m/z 375 to

1500) was acquired in the Orbitrap analyzer at a nominal resolution of 120,000. The automatic gain control (AGC) target was set as 100% standard, with the maximum injection time of 50 ms. The most abundant ions in charge states 2^+ to 7^+ were isolated in a 3 s cycle, fragmented using HCD MS/MS with 33% normalized collision energy, and detected in the Orbitrap analyzer at a nominal mass resolution of 50,000. The AGC target for MS/MS was set as 250% standard with a maximum injection time of 100 ms, whereas dynamic exclusion was set to 45 s with a 10-ppm mass window.

Bottom-up proteomics data analysis

Analysis of nanoLC-MS fractions was carried out using Proteome Discoverer 3.1 (Thermo Scientific) with database search against the full Uniprot human protein database UP000005640 for peptide and protein identification and quantification. Datasets were normalized on total TMT ion reporter intensity and on the average of DMSO controls, to obtain the final values soluble amount variation of each protein and relative statistical significance of variation by P-values calculated by student's t-test across their biological triplicates.

Statistical Analysis

For peptide-level data, statistical significance between groups was assessed using Student's t-test. At the protein level, enrichment analysis was performed using Fisher's exact test, where the top three peptides per protein were selected based on a combined score calculated as the absolute value of the log2 fold change multiplied by the negative log10 of the p-value ($|\log2FC| \times -\log10\ p$). All statistical analyses were conducted using R (version 4.5.0). A p-value threshold of < 0.05 was considered statistically significant.

Ligand–Protein Interaction Mapping with PyMOL.

To characterize the interactions between the proteins and the ligand staurosporine or rapamycin, we retrieved the crystal structure of the complex using PyMOL. The protein was visualized in cartoon representation and colored slate, while the Rapamycin molecule was shown as sticks and colored orange. Protein residues within 4 Å of the ligand were identified as the binding site and displayed as cyan sticks. Hydrogen bonds (≤3.5 Å) between Rapamycin and the protein were visualized as red dashed lines. Hydrophobic interactions were mapped by identifying protein carbon atoms within 4 Å of the ligand, shown in yellow. Charged interactions were identified by selecting positively charged residues (Lys, Arg, His) and negatively charged residues (Asp, Glu) in proximity (≤4 Å) to polar atoms (N and O) on the ligand; these were

displayed in magenta, and associated salt bridges were rendered as magenta dashed lines. Residues near the ligand were labeled for clarity. An embedded Python script iterated over each interaction type to generate a tab-delimited file listing the interacting residues, their chain ID, residue number, and interaction type.

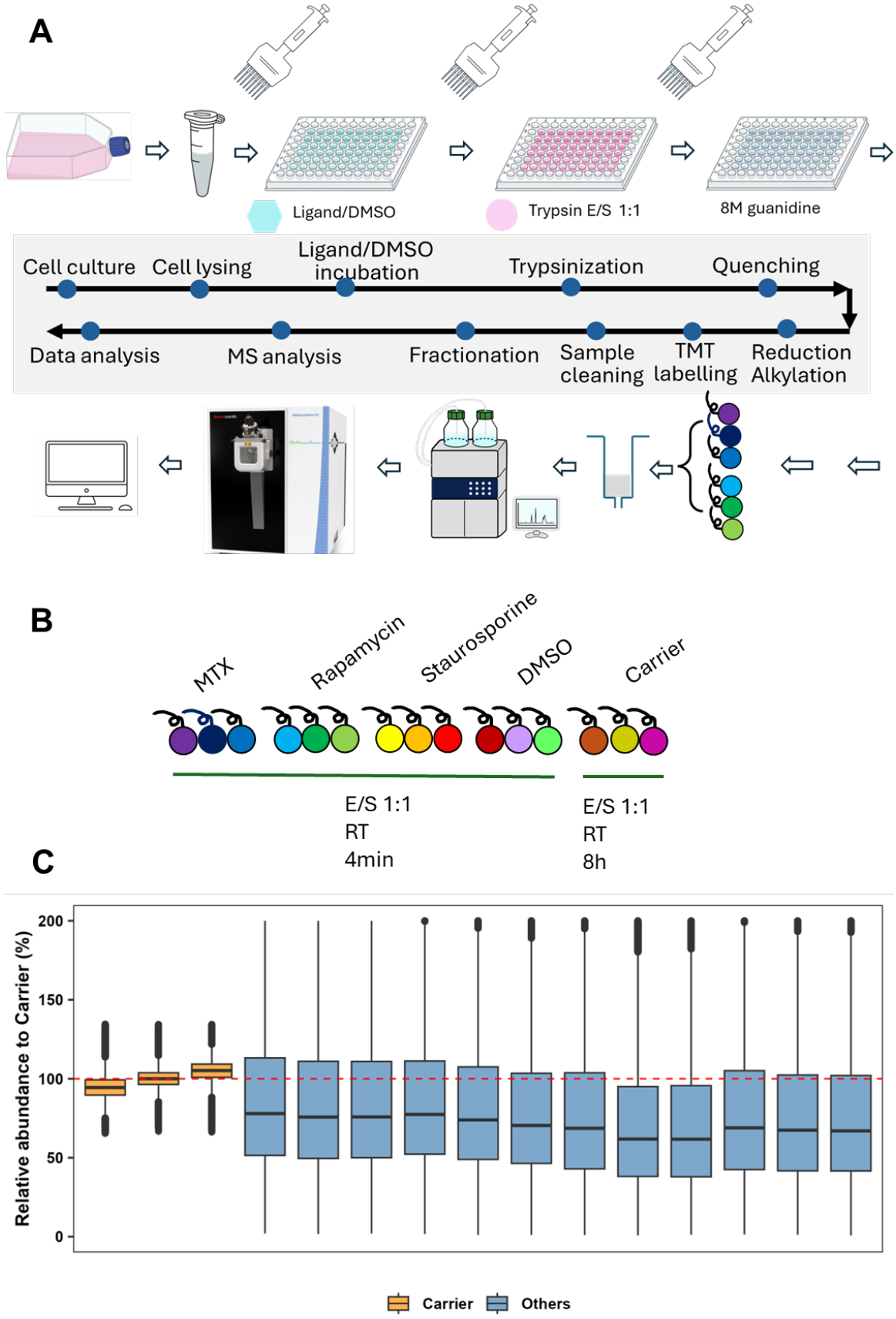

Figure 1 | Overview of Experimental Workflow and TMT Labeling.
A, Workflow of HOLSE. E/S ratio (wt/wt).

B, TMT labeling scheme showing the assignment of unique tags to samples from different experimental groups and the inclusion of Carrier channels.
C, Box plot showing relative peptide abundance for each TMT channel normalized to the carrier (dashed line at 100%)

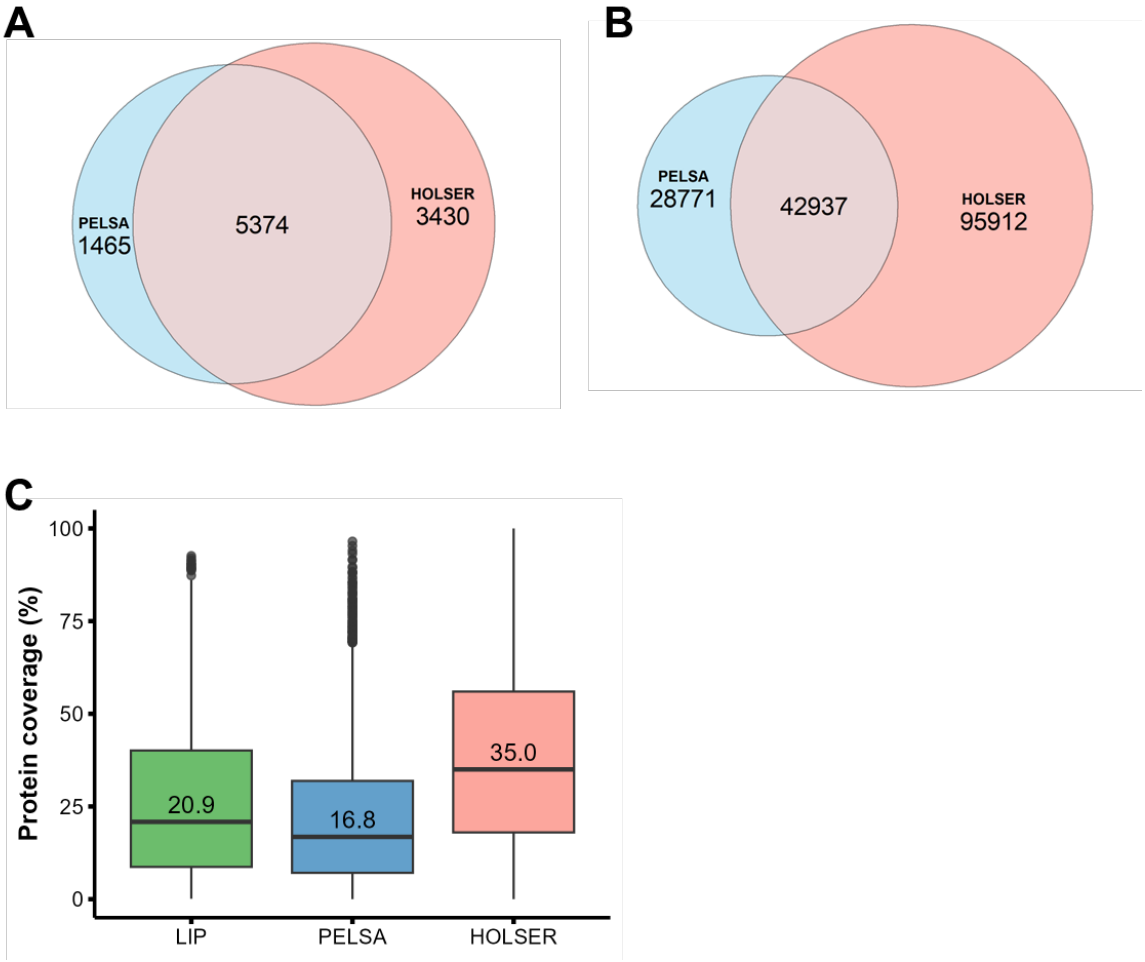

Figure 2 | Comparison of HOLSE and PELSA performance.

A, Venn diagram showing the overlap in quantified proteins between HOLSE and PELSA experiments.

B, Venn diagram illustrating the overlap in quantified peptides between HOLSE and PELSA experiments.

C, Box plot comparing protein sequence coverage across different experimental conditions.

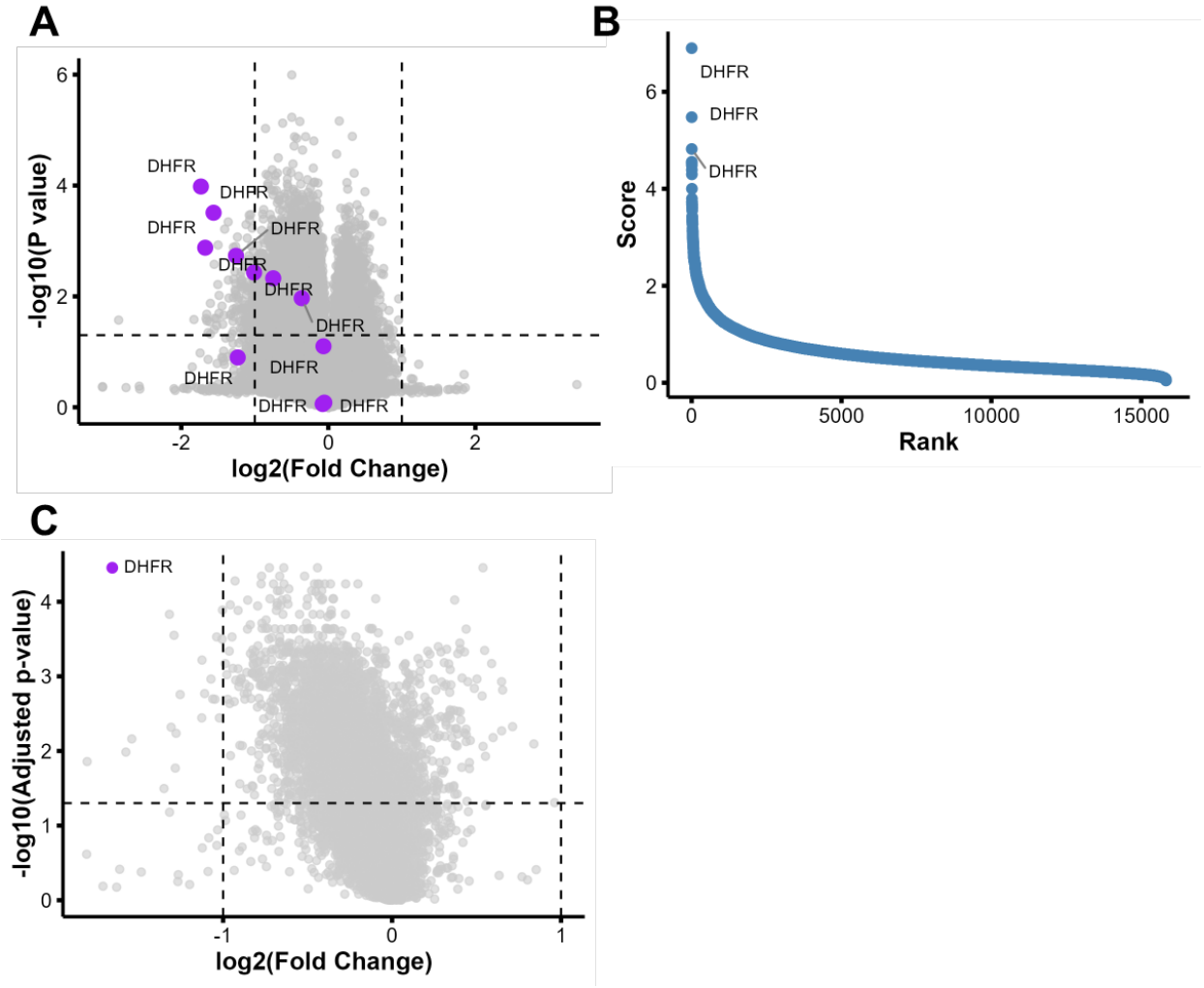

Figure 3 | Peptide and protein abundance changes upon MTX treatment.
A, Volcano plot displaying peptide abundance changes in MTX-treated samples compared with DMSO controls (n=3 biological replicates). Peptides derived from DHFR are highlighted in purple. Statistical significance was assessed by t-test.
B, Ranked list of peptides according to their combined score (absolute log2 fold change × – log10 p-value) calculated from replicate data.
C, Volcano plot showing protein-level abundance changes in MTX-treated samples compared with DMSO controls (n=3 biological replicates). Statistical significance was assessed by t-test.

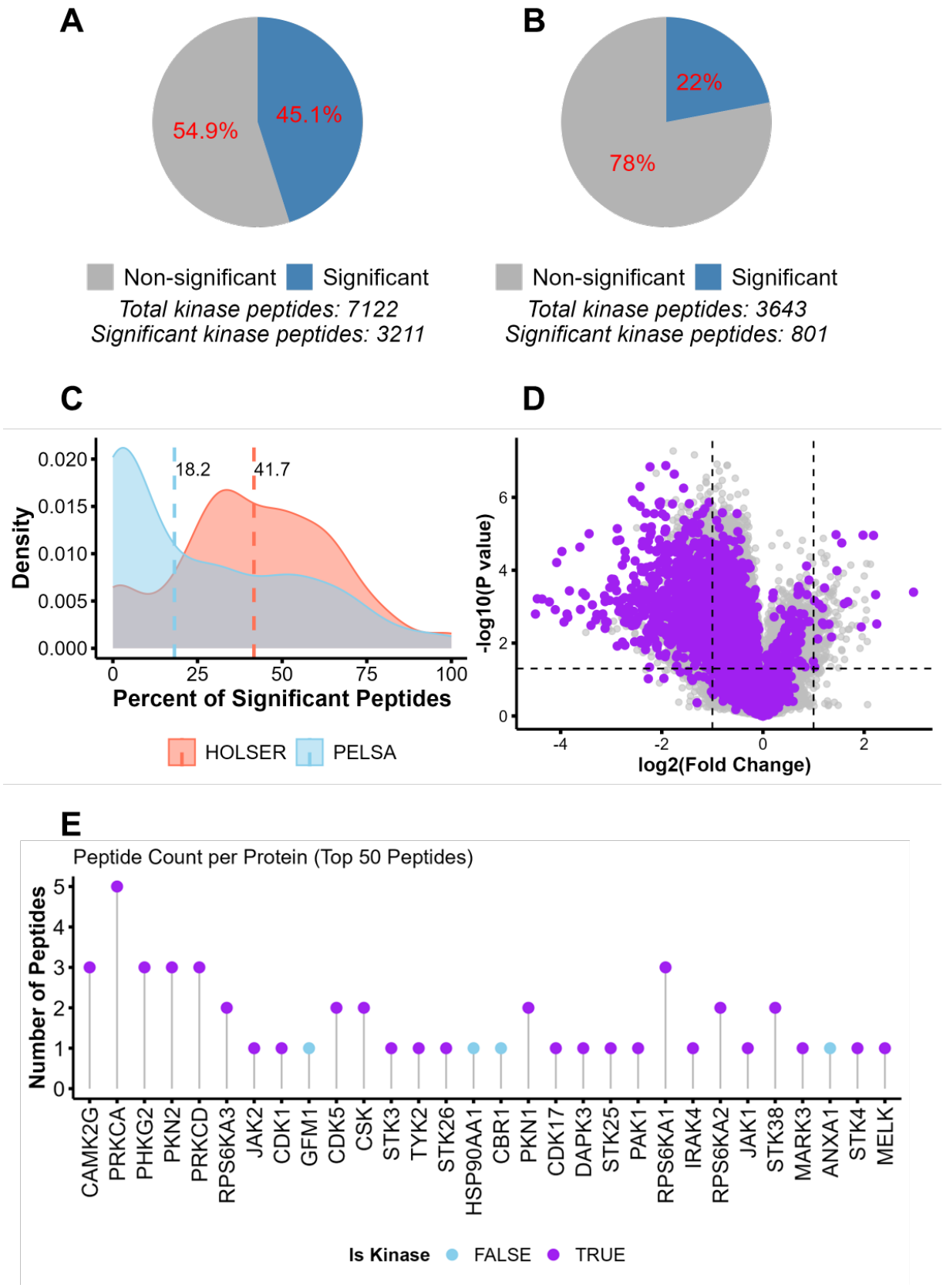
A
54.9%
45.1%
Non-significant
Significant
Total kinase peptides: 7122
Significant kinase peptides: 3211
B
22%
78%
Non-significant
Significant
Total kinase peptides: 3643
Significant kinase peptides: 801
C
Density
0.020
0.015
0.010
0.005
0.000
18.2
41.7
0
25
50
75
100
Percent of Significant Peptides
HOLSER
PELSA
D
-log10(P value)
6
4
2
0
-4
-2
0
2
log2(Fold Change)
E
Peptide Count per Protein (Top 50 Peptides)
Number of Peptides
5
4
3
2
1
0
CAMK2G
PRKCA
PHKG2
PKN2
PRKCD
RPS6KA3
JAK2
CDK1
GFM1
CDK5
CSK
STK3
TYK2
STK26
HSP90AA1
CBR1
PKN1
CDK17
DAPK3
STK25
PAK1
RPS6KA1
IRAK4
RPS6KA2
JAK1
STK38
MARK3
ANXA1
STK4
MELK
Is Kinase
FALSE
TRUE

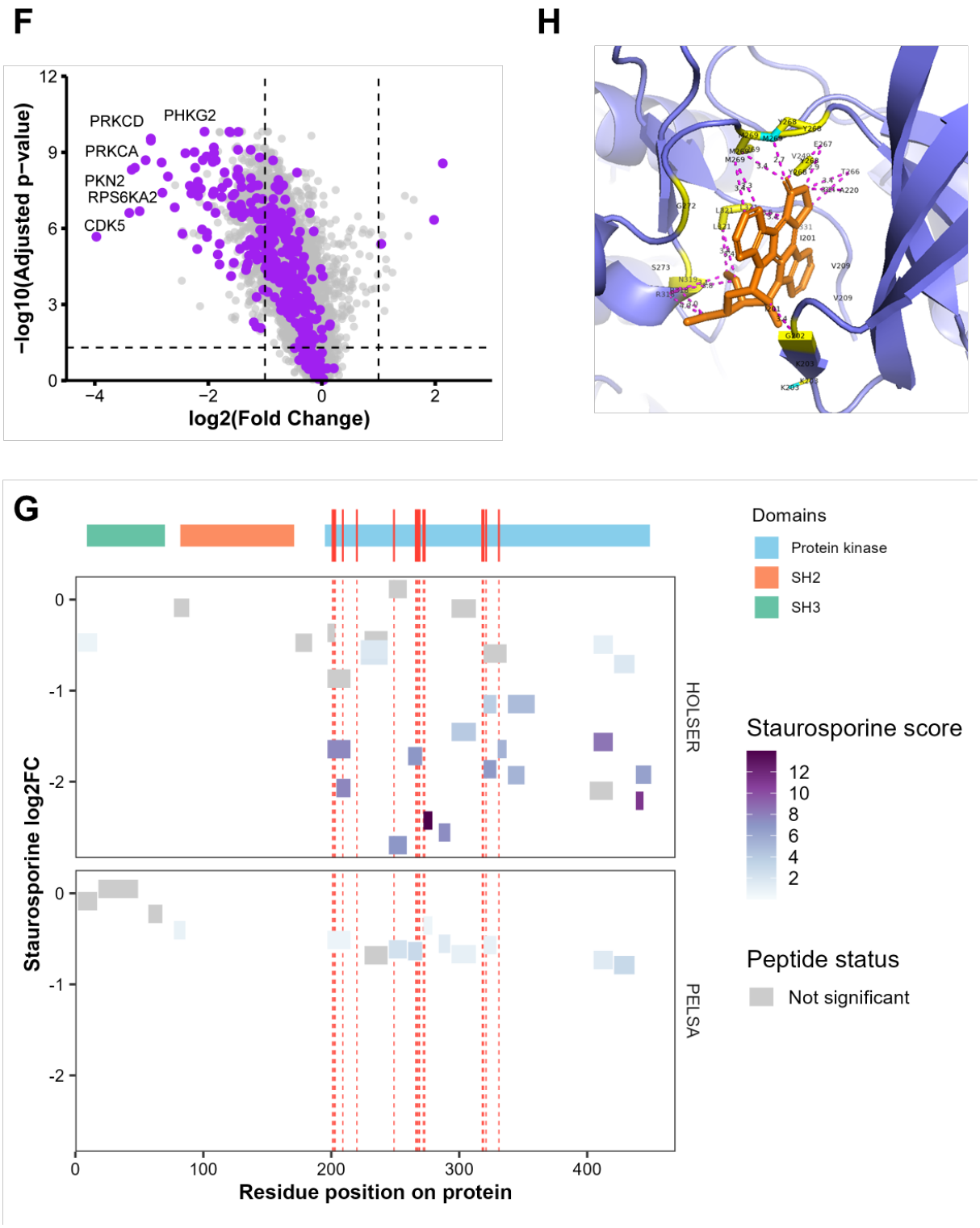

Figure 4 | Kinase-targeting analysis using HOLSE and PELSA.

A, Percentage of kinase-derived peptides (UniProt annotation) showing significant abundance changes ($p < 0.05$, t-test, n = 3 biological replicates) in HOLSER.

B, Percentage of significant kinase-derived peptides ($p < 0.05$, t-test, n = 4 biological replicates) in PELSA.

C, Density plot showing the distribution of significant peptide percentages per kinase in HOLSER and PELSA. Dashed lines indicate the median values for each method.

D, Volcano plot displaying peptide-level abundance changes in staurosporine-treated samples compared with DMSO controls (n = 3 biological replicates). Peptides annotated to kinases are highlighted in purple. Statistical significance was assessed by t-test.
E, Bar plot showing proteins corresponding to the top 50 peptides ranked by score. The number of peptides identified per protein is indicated.
F, Volcano plot showing protein-level abundance changes in staurosporine-treated samples compared with DMSO controls (n = 3 biological replicates). Proteins annotated as kinases are highlighted in purple. Statistical significance was assessed by t-test.
G, Mapping of CSK-derived peptides identified in HOLSE and PELSA onto the protein sequence.
H, Structural visualization of the CSK–substrate complex based on the crystal structure (PDB ID: 1BYG), rendered in PyMOL.

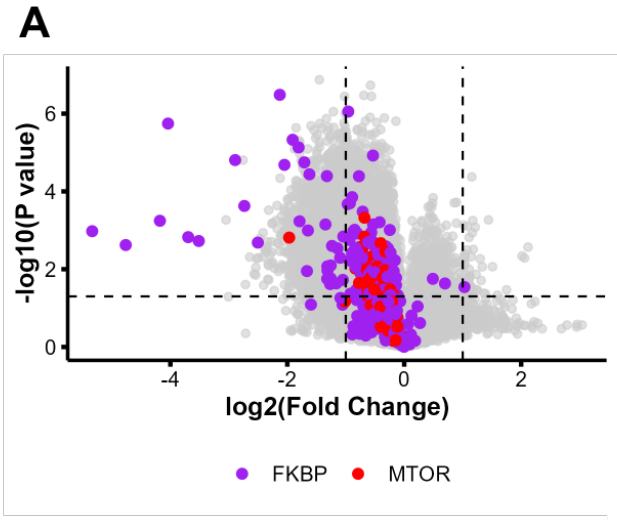
A
-log10(P value)
log2(Fold Change)
FKBP
MTOR

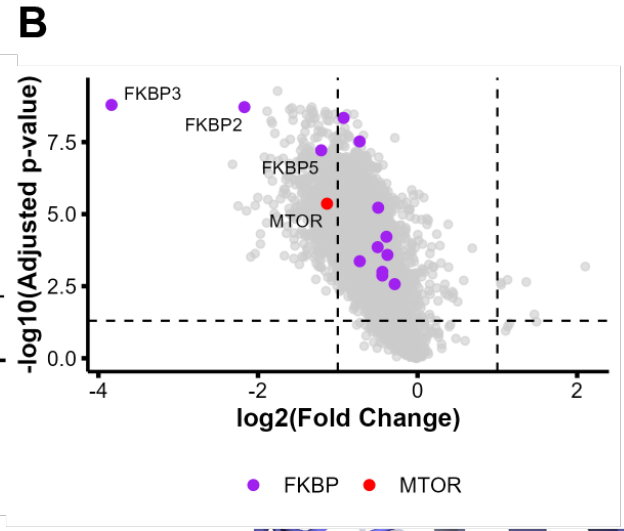
B
FKBP3
FKBP2
FKBP5
MTOR
-log10(Adjusted p-value)
log2(Fold Change)
FKBP
MTOR

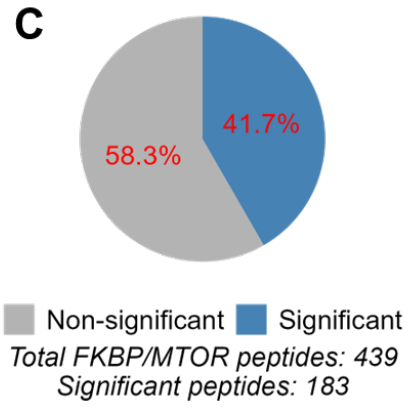
C
41.7%
58.3%
Non-significant
Significant
Total FKBP/MTOR peptides: 439
Significant peptides: 183

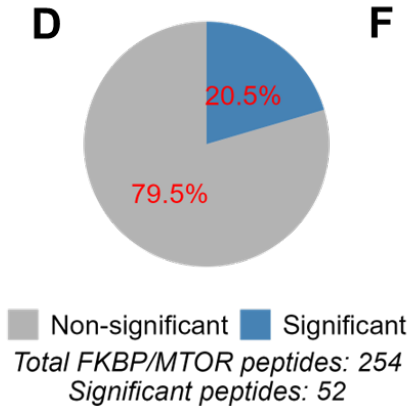
D
20.5%
79.5%
Non-significant
Significant
Total FKBP/MTOR peptides: 254
Significant peptides: 52

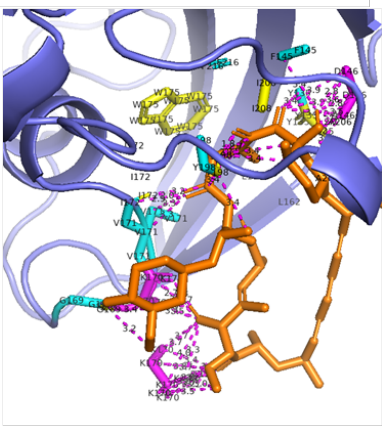
F

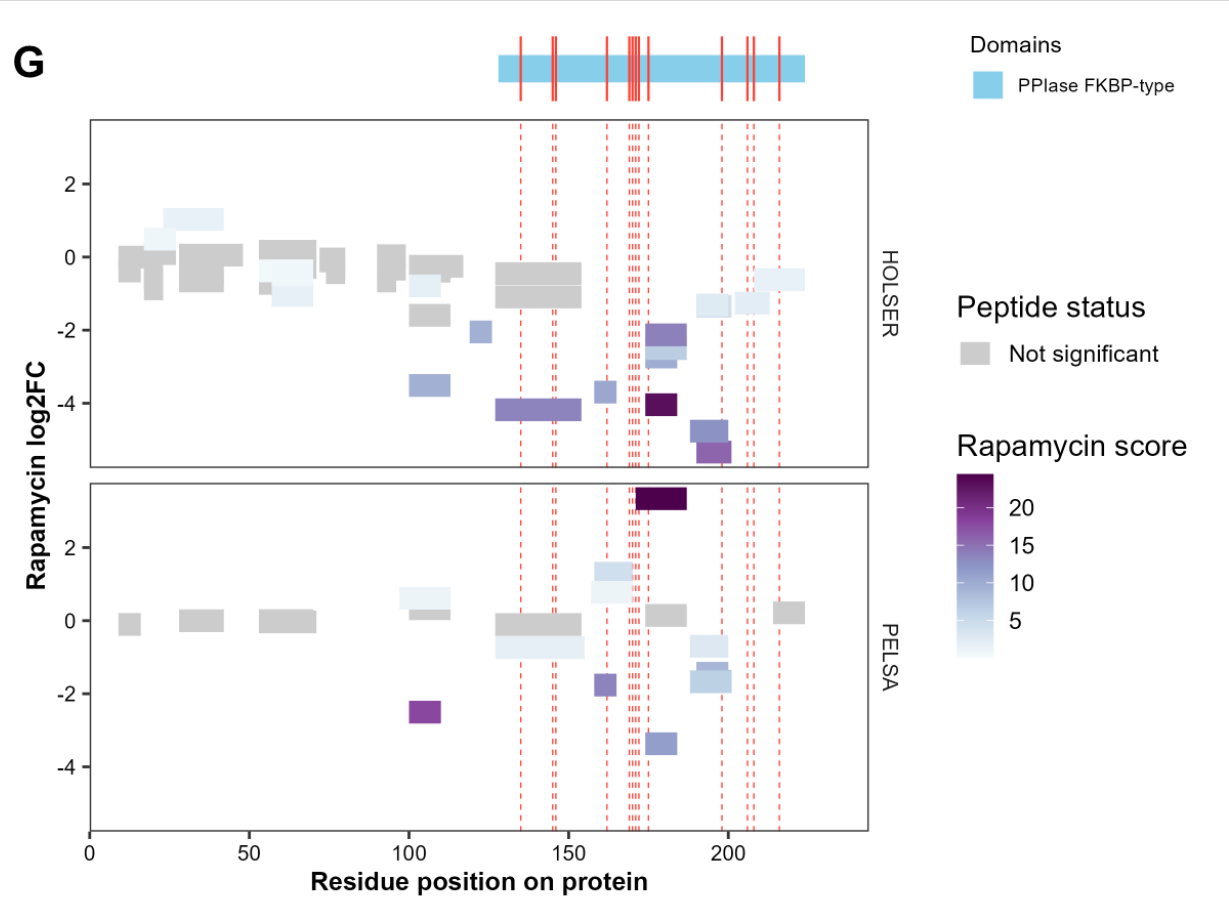
G
Domains
PPIase FKBP-type
HOLSER
PELSA
Rapamycin log2FC
Residue position on protein
Peptide status
Not significant
Rapamycin score
20
15
10
5

Figure 5 | FKBP and mTOR response to rapamycin treatment.
Volcano plot displaying peptide-level (**A**) and protein-level (**B**) abundance changes in rapamycin-treated samples compared with DMSO controls (n = 3 biological replicates). Peptides/proteins annotated to the FKBP family and mTOR are highlighted in purple. Statistical significance was assessed by t-test.
C, Percentage of FKBP- and mTOR-derived peptides showing significant abundance changes ($p < 0.05$, t-test, n = 3 biological replicates) in HOLSER.
D, Percentage of FKBP- and mTOR-derived peptides showing significant abundance changes ($p < 0.05$, t-test, n = 4 biological replicates) in PELSA.
E, Mapping of FKBP3-derived peptides identified in HOLSE and PELSA onto the protein sequence.
F, Structural visualization of the FKBP3–substrate complex based on the crystal structure (PDB ID: 1PBK), rendered in PyMOL.

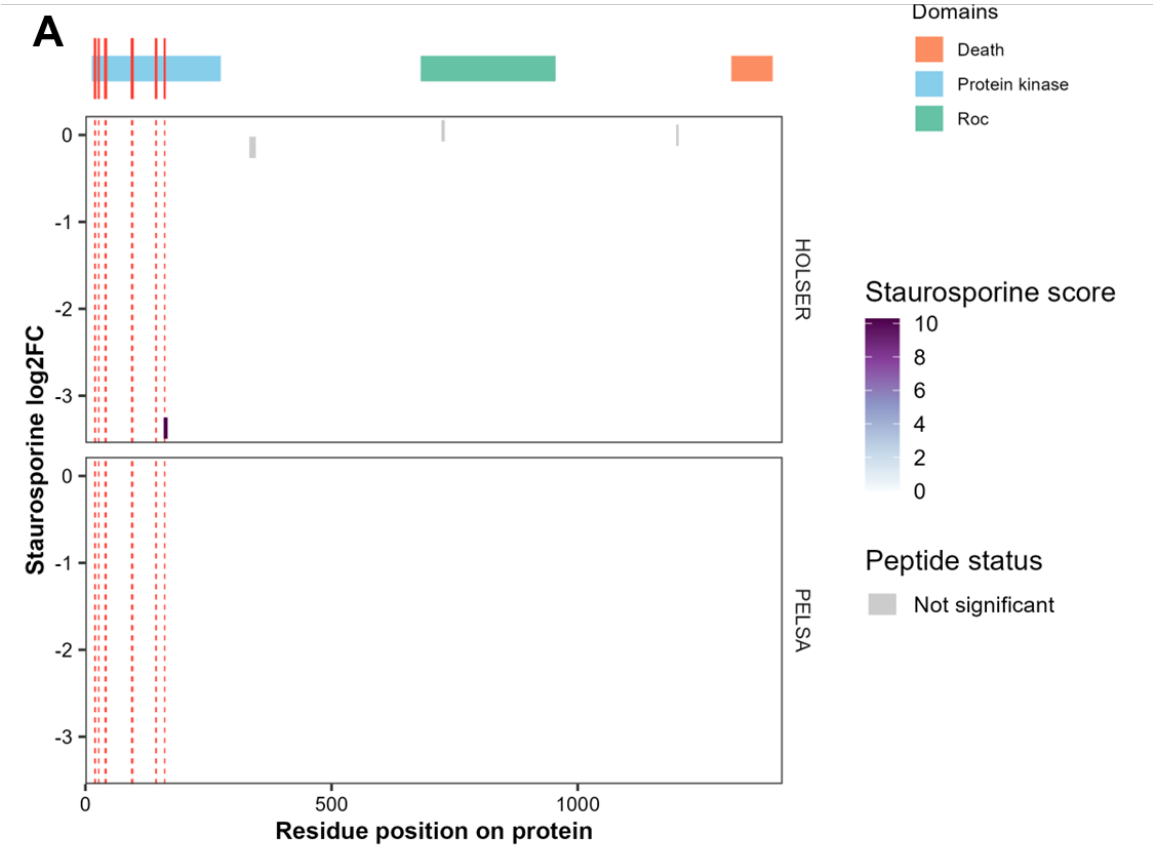
A
Domains
Death
Protein kinase
Roc
Staurosporine score
10
8
6
4
2
0
Peptide status
Not significant
HOLSER
PELSA
Staurosporine log2FC
0
-1
-2
-3
0
500
1000
Residue position on protein

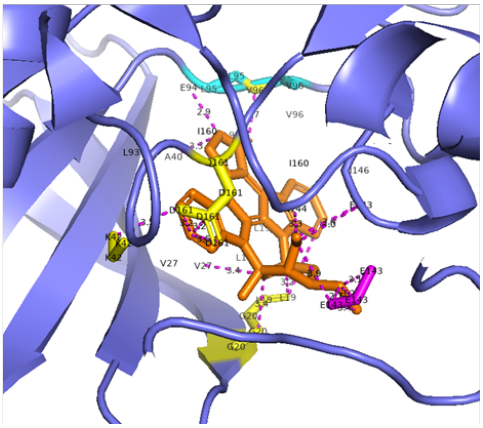
B

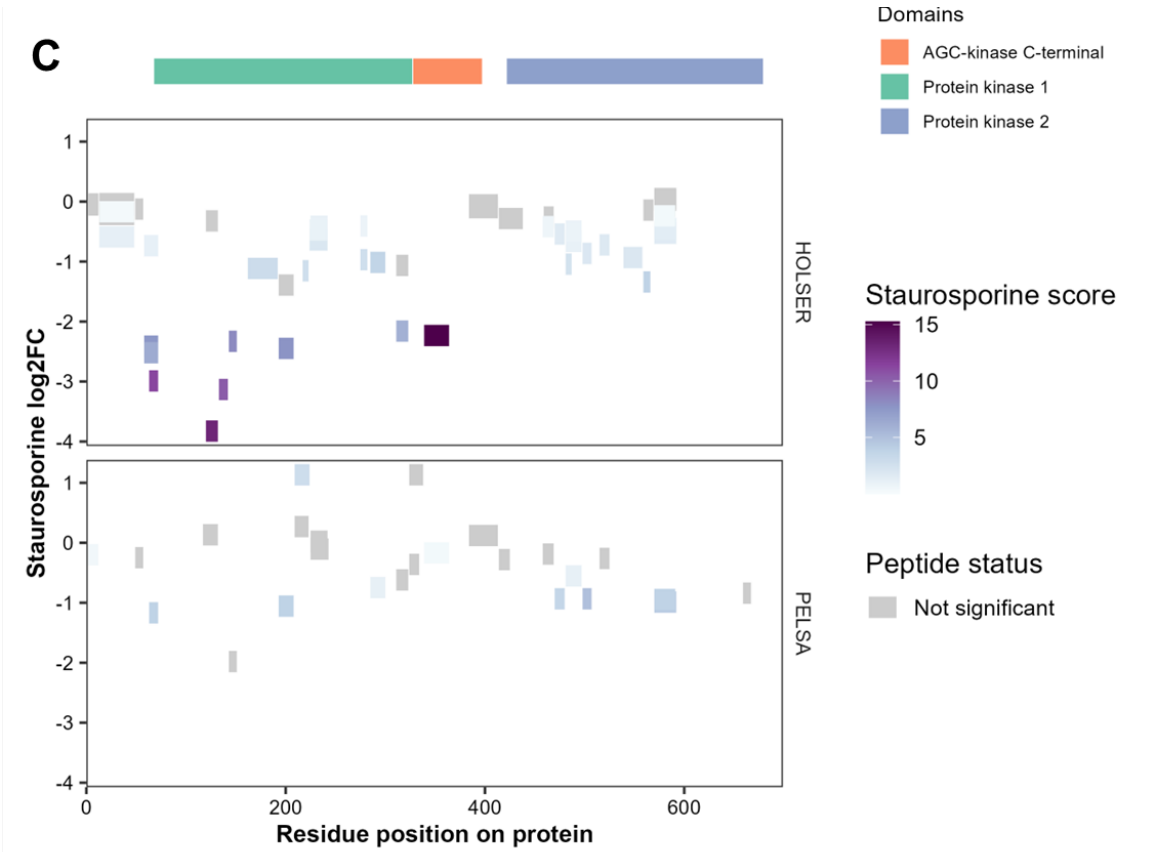

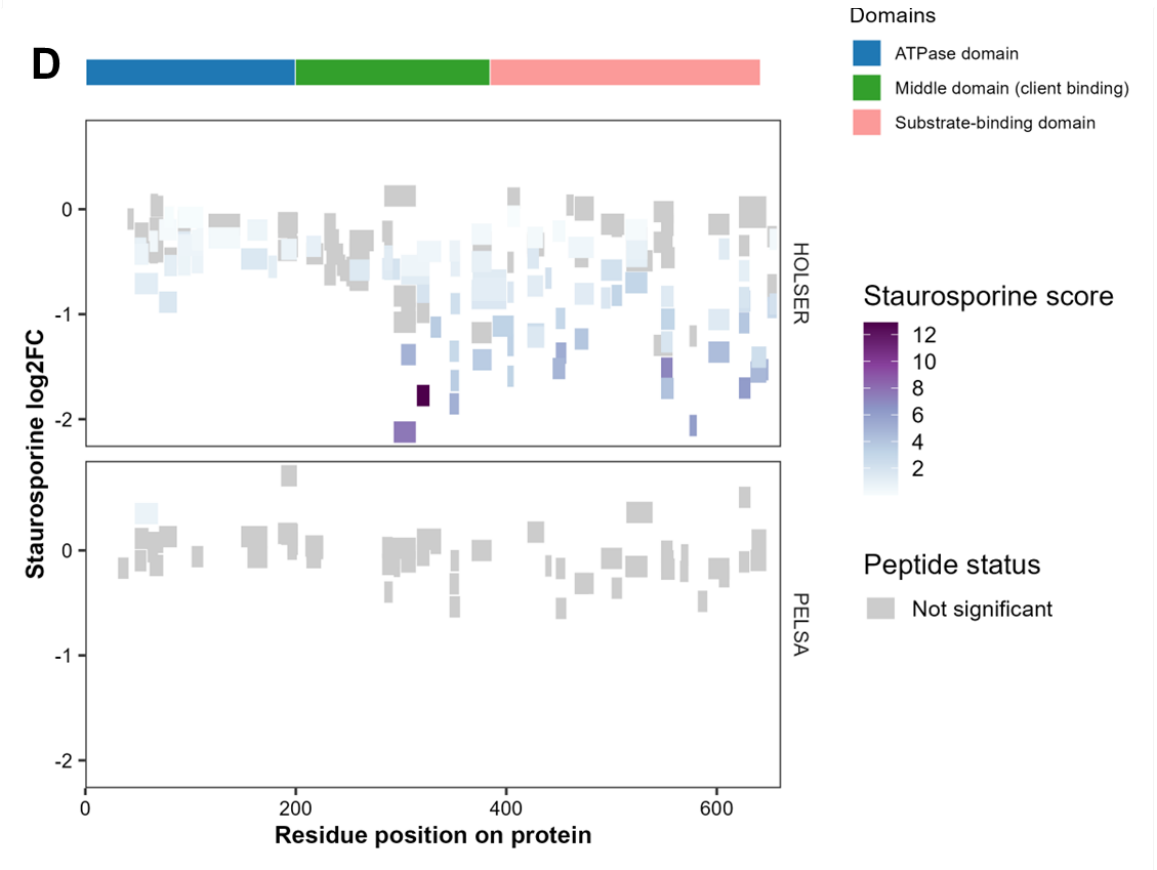

Supplementary Figure 1 | A, Mapping of DAKP1-derived peptides identified in HOLSE and PELSA onto the protein sequence. **B,** Structural visualization of the DAKP1–substrate

complex based on the crystal structure (PDB ID: 1WVY), rendered in PyMOL. Mapping of RPS6KA3 (**C**) and HAP90AA1 (**D**)-derived peptides identified in HOLSE and PELSA onto the protein sequence.

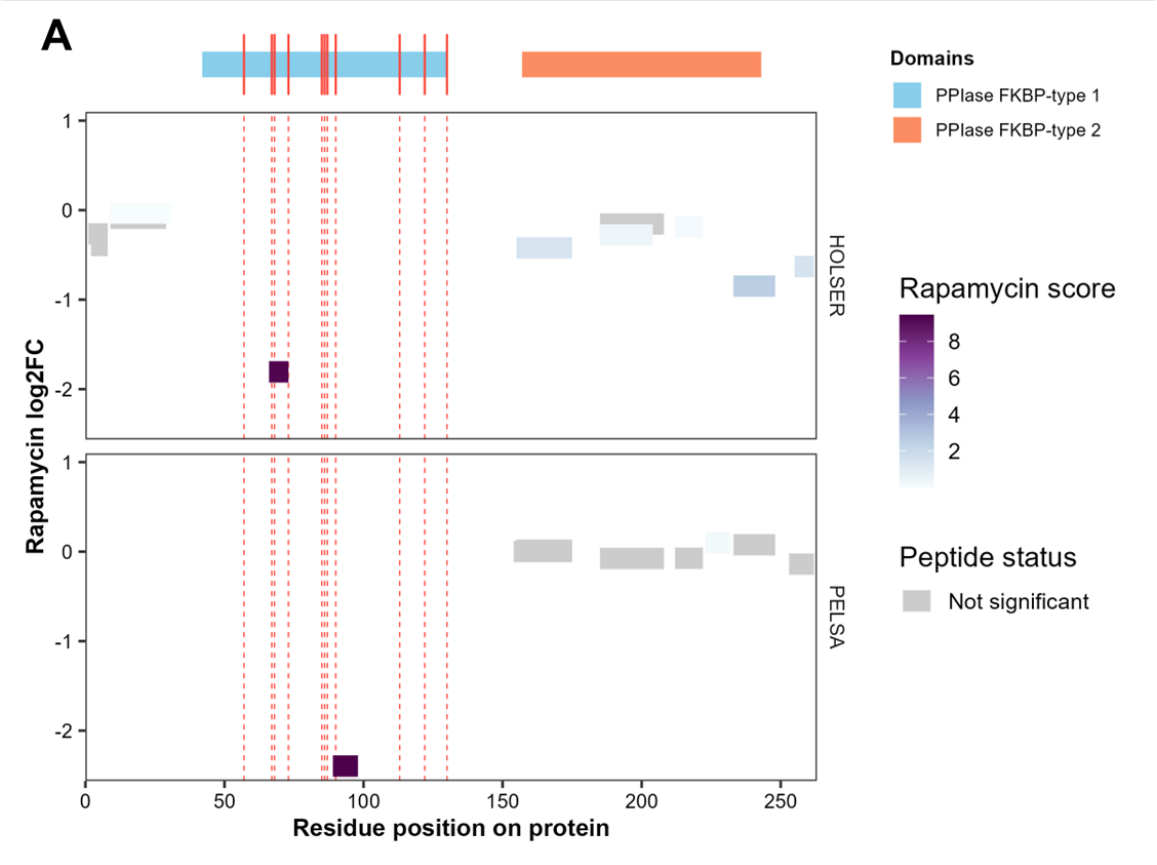
A
Domains
PPIase FKBP-type 1
PPIase FKBP-type 2
Rapamycin score
8
6
4
2
Peptide status
Not significant
HOLSER
PELSA
Rapamycin log2FC
1
0
-1
-2
0
50
100
150
200
250
Residue position on protein

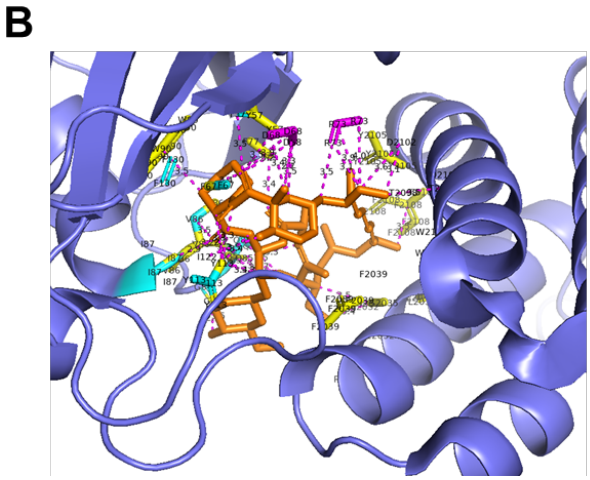
B

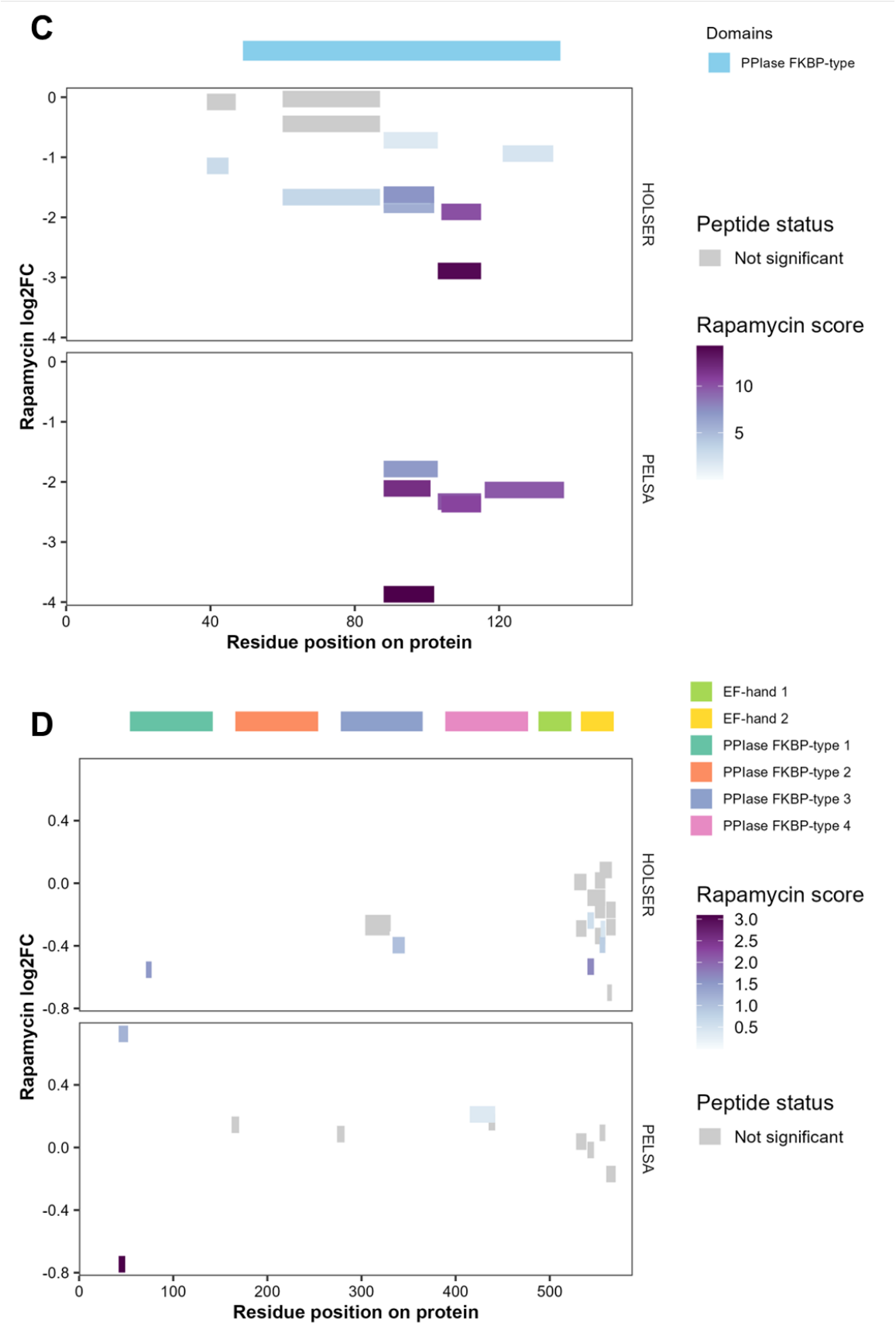

Supplementary Figure 2 | A, Mapping of FKBP5-derived peptides identified in HOLSE and PELSA onto the protein sequence. **B,** Structural visualization of the FKBP5–substrate

complex based on the crystal structure (PDB ID: 4DRI), rendered in PyMOL. Mapping of FKBP2 (**C**) and FKBP9 (**D**)-derived peptides identified in HOLSE and PELSA onto the protein sequence.

References

1. Schopper, S., Kahraman, A., Leuenberger, P., Feng, Y., Piazza, I., Müller, O., Boersema, P.J. & Picotti, P. Measuring protein structural changes on a proteome-wide scale using limited proteolysis-coupled mass spectrometry. *Nat. Protoc.* **12**, 2391-2410 (2017).
2. Piazza, I., Kochanowski, K., Cappelletti, V., Fuhrer, T., Noor, E., Sauer, U. & Picotti, P. A Map of Protein-Metabolite Interactions Reveals Principles of Chemical Communication. *Cell* **172**, 358-372.e323 (2018).
3. Feng, Y., De Franceschi, G., Kahraman, A., Soste, M., Melnik, A., Boersema, P.J., de Laureto, P.P., Nikolaev, Y., Oliveira, A.P. & Picotti, P. Global analysis of protein structural changes in complex proteomes. *Nat. Biotechnol.* **32**, 1036-1044 (2014).
4. Li, K., Chen, S., Wang, K., Wang, Y., Xue, L., Ye, Y., Fang, Z., Lyu, J., Zhu, H., Li, Y., Yu, T., Yang, F., Zhang, X., Guo, S., Ruan, C., Zhou, J., Wang, Q., Dong, M., Luo, C. & Ye, M. A peptide-centric local stability assay enables proteome-scale identification of the protein targets and binding regions of diverse ligands. *Nat. Methods* **22**, 278-282 (2025).
5. Végvári, Á., Rodriguez, J.E. & Zubarev, R.A. Single-Cell Chemical Proteomics (SCCP) Interrogates the Timing and Heterogeneity of Cancer Cell Commitment to Death. *Anal. Chem.* **94**, 9261-9269 (2022).
6. Lawrie, A.M., Noble, M.E., Tunnah, P., Brown, N.R., Johnson, L.N. & Endicott, J.A. Protein kinase inhibition by staurosporine revealed in details of the molecular interaction with CDK2. *Nat. Struct. Biol.* **4**, 796-801 (1997).
7. Yanagihara, N., Tachikawa, E., Izumi, F., Yasugawa, S., Yamamoto, H. & Miyamoto, E. Staurosporine: An Effective Inhibitor for Ca2+/Calmodulin-Dependent Protein Kinase II. **56**, 294-298 (1991).
8. Whitesell, L. & Lindquist, S.L. HSP90 and the chaperoning of cancer. *Nat. Rev. Cancer* **5**, 761-772 (2005).
9. Taipale, M., Jarosz, D.F. & Lindquist, S. HSP90 at the hub of protein homeostasis: emerging mechanistic insights. *Nat. Rev. Mol. Cell Biol.* **11**, 515-528 (2010).
10. Weyd, H., Abeler-Dörner, L., Linke, B., Mahr, A., Jahndel, V., Pfrang, S., Schnölzer, M., Falk, C.S. & Krammer, P.H. Annexin A1 on the surface of early apoptotic cells suppresses CD8+ T cell immunity. *PLoS One* **8**, e62449 (2013).
11. Blume, K.E., Soeroes, S., Keppeler, H., Stevanovic, S., Kretschmer, D., Rautenberg, M., Wesselborg, S. & Lauber, K. Cleavage of annexin A1 by ADAM10 during secondary necrosis generates a monocytic "find-me" signal. *J. Immunol.* **188**, 135-145 (2012).
12. Karaman, M.W., Herrgard, S., Treiber, D.K., Gallant, P., Atteridge, C.E., Campbell, B.T., Chan, K.W., Ciceri, P., Davis, M.I., Edeen, P.T., Faraoni, R., Floyd, M., Hunt, J.P., Lockhart, D.J., Milanov, Z.V., Morrison, M.J., Pallares, G., Patel, H.K., Pritchard, S., Wodicka, L.M. & Zarrinkar, P.P. A quantitative analysis of kinase inhibitor selectivity. *Nat. Biotechnol.* **26**, 127-132 (2008).
13. Lamers, M.B., Antson, A.A., Hubbard, R.E., Scott, R.K. & Williams, D.H. Structure of the protein tyrosine kinase domain of C-terminal Src kinase (CSK) in complex with staurosporine. *J. Mol. Biol.* **285**, 713-725 (1999).

14. Davies, S.P., Reddy, H., Caivano, M. & Cohen, P. Specificity and mechanism of action of some commonly used protein kinase inhibitors. *Biochem. J* **351**, 95-105 (2000).
15. März, A.M., Fabian, A.K., Kozany, C., Bracher, A. & Hausch, F. Large FK506-binding proteins shape the pharmacology of rapamycin. *Mol. Cell. Biol.* **33**, 1357-1367 (2013).
16. Saxton, R.A. & Sabatini, D.M. mTOR Signaling in Growth, Metabolism, and Disease. *Cell* **168**, 960-976 (2017).
17. Jin, Y.J., Burakoff, S.J. & Bierer, B.E. Molecular cloning of a 25-kDa high affinity rapamycin binding protein, FKBP25. *J. Biol. Chem.* **267**, 10942-10945 (1992).
18. Liang, J., Hung, D.T., Schreiber, S.L. & Clardy, J. Structure of the Human 25 kDa FK506 Binding Protein Complexed with Rapamycin. *J. Am. Chem. Soc.* **118**, 1231-1232 (1996).
19. Sinars, C.R., Cheung-Flynn, J., Rimerman, R.A., Scammell, J.G., Smith, D.F. & Clardy, J. Structure of the large FK506-binding protein FKBP51, an Hsp90-binding protein and a component of steroid receptor complexes. *Proc. Natl. Acad. Sci. U. S. A.* **100**, 868-873 (2003).
20. Kumar, S. & Nussinov, R. Salt bridge stability in monomeric proteins11Edited by J. M. Thornton. *J. Mol. Biol.* **293**, 1241-1255 (1999).
21. Donald, J.E., Kulp, D.W. & DeGrado, W.F. Salt bridges: Geometrically specific, designable interactions. **79**, 898-915 (2011).
22. Bogan, A.A. & Thorn, K.S. Anatomy of hot spots in protein interfaces11Edited by J. Wells. *J. Mol. Biol.* **280**, 1-9 (1998).
23. Janin, J., Miller, S. & Chothia, C. Surface, subunit interfaces and interior of oligomeric proteins. *J. Mol. Biol.* **204**, 155-164 (1988).
24. Young, T., Abel, R., Kim, B., Berne, B.J. & Friesner, R.A. Motifs for molecular recognition exploiting hydrophobic enclosure in protein-ligand binding. *Proc. Natl. Acad. Sci. U. S. A.* **104**, 808-813 (2007).
25. Göthel, S.F. & Marahiel, M.A. Peptidyl-prolyl cis-trans isomerases, a superfamily of ubiquitous folding catalysts. *Cell. Mol. Life Sci.* **55**, 423-436 (1999).
26. Jo, D., Lyu, M.S., Cho, E.G., Park, D., Kozak, C.A. & Kim, M.G. Identification and genetic mapping of the mouse Fkbp9 gene encoding a new member of FK506-binding protein family. *Mol. Cells* **12**, 272-275 (2001).